IEEE Access
Multidisciplinary | Rapid Review | Open Access Journal

Received August 11, 2019, accepted August 26, 2019, date of publication September 13, 2019, date of current version September 30, 2019.

Digital Object Identifier 10.1109/ACCESS.2019.2941253

Design and Optimization of a Homopolar Permanent-Magnet Linear Tubular Motor Equipped With the E-Core Stator

YU ZOU AND KA WAI ERIC CHENG, (Senior Member, IEEE)
Power Electronics Research Center, Department of Electrical Engineering, The Hong Kong Polytechnic University, Hong Kong
Corresponding author: Ka Wai Eric Cheng (eric-cheng.cheng@polyu.edu.hk)

ABSTRACT In this study, a new homopolar permanent-magnet (PM) linear tubular motor is designed, analyzed and optimized. Firstly, a mechanical structure of the linear oscillating motor (LOM) is proposed and the main working principles are introduced. A basic dynamic mathematic model of the motor is given. Secondly, the magnetic circuit of the motor is analyzed and equivalent magnetic modes are obtained to estimate the magnetic characteristic and force outputs. Thirdly, optimizations including the tooth stricter of the E-core stator, the size of the PM and the air gap length are carried out to improve the force output performance of the motor, increasing force outputs and reducing force ripples during the stroke. Finally, the motor prototype is manufactured according to the design and experimental tests involving force outputs and working efficiency are measured. The average force output and efficiency of the motor can achieve 60 N and 67 %, respectively. Results obtained by finite element method (FEM) and experiments prove the correctness of the design and the effectiveness of the LOM.

INDEX TERMS FEM, homopolar PM, LOM, optimization.

I. INTRODUCTION

Linear oscillatory motors (LOMs) are extensively employed in industrial applications and domestic appliances, such as wire bonders, air conditioners and refrigerators and so on. High-frequency oscillations are necessary for these applications. Generally, some tubular LOMs can provide a high-frequency reciprocating movement and they usually move less than one pole pitch of the whole stroke. In literature [1], a linear tubular switched reluctance compressor is designed and tested in a refrigerator. Switched reluctance motors, however, have low efficiency and less force to volume ratio compared with permanent magnet (PM) motors, which means they are usually operated with low power density. Consequently, this compressor has a relatively big volume and a small power density. In order to address this problem, linear PM oscillating motors are usually investigated by researchers before. For PM LOMs, iron core and coreless approaches are developed for diverse applications. In [2], a voice coil vibration motor is designed with moving magnets. The movement is limited by PMs at the end of the motor. Thus, the moving displacement will be also limited and this motor is only used in short stroke oscillation. Apart from moving PMs, the mover consist of coils in the motor has been designed, with armature reaction analyzed in [3]. Some PMs are optimized for linear motors to improve their performance in [4], [5]. Also, some LOMs with an iron core have also been developed recently and there are two classifications for different core shapes including C-core and E-core, respectively. A C-core LOM is investigated for different laminated stators in [6] and different PMs are also developed in [7]. This type of LOM is usually used in linear compressors with less moving displacement. In [8], a C-core LOM with Halbach magnets mover is designed. The efficiency and iron loss of the motor is analyzed. Results show that the efficiency of the motor can exceed 92%. Meanwhile, the E-core LOMs are presented by a series investigation in [9]–[14]. There are mainly four types of PM LOMs involving an E-core stator, as shown in Figure 1. Two coils are embraced by the E-core and connected in anti-series, constructing the windings of the stator. In Figure 1(a), two PM rings magnetized radically are mounted on the surface of the moving part, forming two poles for the motor. This kind of motor could be manufactured easily and it can be produced massively. Similarly, four PM rings are mounted

The associate editor coordinating the review of this manuscript and approving it for publication was Gaolin Wang.

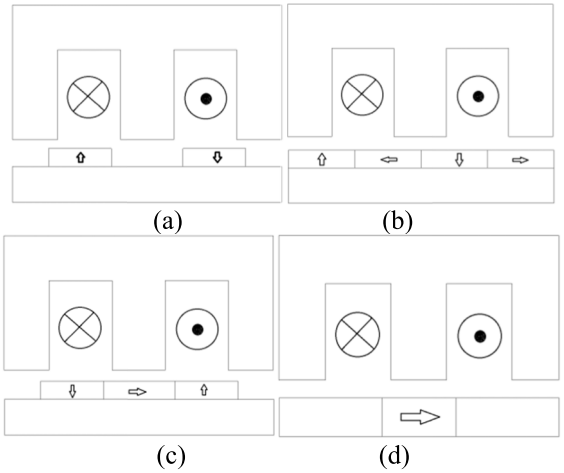

FIGURE 1. The structures of the LOMs with an E-core.(a) Two magnetic rings are magnetized radically. (b) Four magnetic rings are arranged in a Halbach array. (c) An axially magnetized ring is sandwiched by two magnetic rings being radically magnetized. (d) An axially magnetized magnet ring is embedded into an iron core of the mover.

on the surface of the mover to construct a quasi Halbach PMs for the motor, as shown in Figure 1 (b). This structure might have a higher force to volume ratio and the thickness of the back iron of the mover can be reduced as the Halbach PM array. The Halbach PM approach is also studied in Figure 1 (c). Three PM rings are mounted on the surface of the mover. Two of them are magnetized in the radial direction and one is magnetized in the axial direction, constructing the Halbach magnetic poles. A PM ring being axially magnetized is sandwiched by an iron core of the mover to produce two poles for the motor, as shown in Figure 1 (d). This approach could reduce the size of the PMs and increase the force output of the motor, but the mass of the moving part could be added as the moving iron core. In addition, some E-core LOMs are designed by transverse flux way and employed by linear compressors. In [15], two types LOMs with transverse flux are compared and the results showed that the thrust of the two methods is very similar. The transverse flux LOMs equipped by PMs and PM free approach are compared in [16]. Consequently, although the LOM with PMs performs better physically according to the research results, the cost and the manufacturing procedure cannot outweigh that of LOM without PMs. To obtain reliable and qualified products, a system-level design optimization is investigated for mass production of motors [17]. Also, a multimode design method has been proposed to obtain optimal dimensions of the motor in paper [18]. Furthermore, the multi-objective optimization method is developed with a sensitivity index [19]. These optimization methods are new trend for motor design in the future.

For all E-core LOMs mentioned above, at least two poles should be produced by two magnets or one magnet with iron cores. Though the movements of the mover need a short-stroke reciprocating motion, the truth is that the displacement is limited by the structure and this kind of structure cannot

TABLE 1. Characteristics of LOMs with E-core stators.

Style	Advantages	Disadvantages
Surface mounted PM	High efficiency, high frequency, easy manufacture,	Short stroke
Halbach PM	High efficiency, high frequency	Short stroke, high cost, hard to manufacture
Embedded PM	Low cost,	Short stroke, Low frequency hard to manufacture
Homopolar PM	Long stroke, High frequency, Easy manufacture, Low cost,	Big force ripple

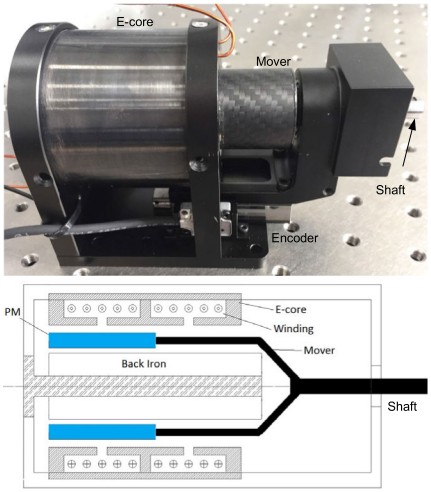

FIGURE 2. Motor prototype and the mechanical section view.

improve the displacement of the moving part because the moving distance is limited in one pole pitch of the motor. These LOMs can be used by linear compressors for air conditioners and refrigerators. They can also be employed by linear vibration motors under high frequency operations for wire bonding equipment.

In this study, a new LOM with an E-core stator is designed. The mechanical structure of the motor is shown in Figure 2(a). Only one homopolar magnet being magnetized radically can the mover be formed for the motor. The moving displacement of the mover can be improved within one stroke. Put it in another way, the moving stroke of the motor cannot be limited in one pole pitch of the motor. The advantages and disadvantages of these linear motors with E-core stators are listed in Table 1. Two coils embraced by the E-core stator can be connected in parallel, series or anti-series on the actual requests and the working mode of the motor can be adjusted according to the requirements. The force output of the mover can be governed precisely by controlling the excitations of the two coils. This paper presents the structure and design procedure of the LOM. The working principles and mechanical construction are introduced in part II. Then, the magnetic

circuit of the motor is designed and analyzed in part III, with FEM vindicated the effectiveness of the designed structure of the magnetic circuit, followed by the optimization of the teeth structure of the E-core stator in part VI. Finally, a prototype of the motor is produced and experimental tests including the force output characteristics, the efficiency with loads for the motor are obtained. Some conclusions end this paper.

II. MECHANICAL STRUCTURE AND BASIC MODEL

A. MECHANICAL STRUCTURE

The mechanical structure of the LOM is shown in Figure 2. The motor mainly consists of the E-core stator, the mover with a PM ring and a shaft. The back iron for the PM is fixed on an aluminum crust of the motor which also embraces the E-core stator. The mover and the stator are connected by a shaft guided by bearings at the end of the mover. The PM ring is mounted on a carbon fiber tube to construct the mover. The mover is installed on a linear guider which is fixed on a basement to ensure the air gap lengths between the stationary part and the mover. The winding of the motor consists of two coils and they can be connected in series with same current-carrying direction shown in Figure 2. Interestingly, the PM ring is magnetized radically regardless of the polarized direction so that only one magnetic pole can produce by the PM for the motor. The magnetic circuit structure of the motor after optimized which will be introduced in part VI as shown in Figure 3 (a). The section view about the ending surface of the motor and the section view along the moving direction are given, including the E-core stator, the PM ring, winding and the back iron. It can be seen that the linear tubular motor has a simple magnetic structure and just a homopolar magnet ring is used to react with the E-core stator after the winding is excited. When changing the coil current direction, the alternative thrust directions along the shaft will push the mover to vibrate. The main advantage of the structure is that the moving distance can be improved under the identical size of the E-core stator, compared with other E-core LOMs. The moving distance can exceed the width of one pole so that the distance can be doubled. In this paper, the moving distance is 25 mm that is longer than other LOMs with the same E-core stator. The E-core stator is made of a soft magnetic powder composite which is comprised by Ni, Fe and Si. The saturated flux density of the material is 1.6 T. The three-dimensional flux distribution generated by the PM is shown in Figure 3 (b). Main flux lines are closed along the E-core stator and the back iron, which suggests that they provide the main magnetic circuit for the motor. The half cross-sectional schematic of the proposed structure is given in Figure 4. There are two air gaps sandwiching the moving magnet. Importantly, the shape of the teeth of the E-core stator plays a significant role in the force ripples of the motor. The length of the gap between the teeth also needs to be designed accurately according to the length of the PM. The main specifications are listed in Table 2.

TABLE 2. Main specifications of the motor.

Symbol	Quantity
Rated power (P)	100W
Rated current of the motor (I)	2 A
Force constant of the motor (k_v)	25
Radium of motor (R_2)	60 mm
Radium of mover (R_1+g_2+t)	17 mm
Stroke length of mover (x)	25 mm
Length of the PM (l)	14 mm
Length of E-core stator (w)	42 mm
Height of the tooth (h_1)	3 mm
Thickness of the PM (t)	2 mm
Thickness of the stator yoke(q)	5 mm
Pole width of the stator (p)	5 mm
Mass of mover (M)	69.8 g
Length of air gap 1 (g_1)	0.3 mm
Length of air gap 2 (g_2)	0.3 mm
Length of open slot (s)	3 mm
Winding turns (N_c)	250
Diameter of coil wire	0.45 mm
Slot filing factor	0.65
Linear encoder accuracy	1 um

B. MATHEMATIC MODEL

For electric terminal of the motor, the dynamic equations can be expressed by

$$V_t = e_j + i_j R_j + L_j \frac{di_j}{dt}, \quad j = 1, 2. \tag{1}$$

where V_t is the terminal voltage of the motor and e is the back electromotive force (EMF). i, R and L are winding current, resistance and inductance, respectively. Lower case symbols denote the windings of the motor. The back-EMFs of the motor can be calculated by

$$e_j = k_v v \tag{2}$$

k_v is the speed constant in the linear direction and v is the speed of the mover. Mechanical output of the motor can be expressed as

$$F = F_l + B_l v + M \frac{dv}{dt} \tag{3}$$

F_l is the load force. B_l is the damping coefficient of the motor. M represents inertia mass of the mover. The electromagnetic force can be calculated by the following equations.

$$F = k_v i \tag{4}$$

The constant k_v is determined by the structure of the motor and the calculation method will be introduced in the magnetic circuit design of the motor.

III. MAGNETIC CIRCUIT DESIGN

The mechanical dimensions of the motor should be estimated according to the magnetic structure, electric load and magnetic load. The mechanical structure and dimensions can be quickly estimated by analyzing the magnetic circuit path. The basic dimensions of motor can be determined if the armature reaction of the motor is considered because the armature

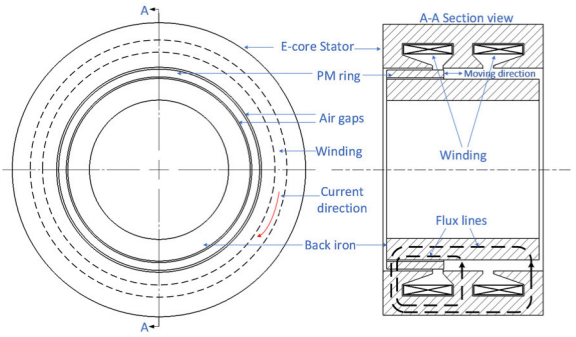

(a)

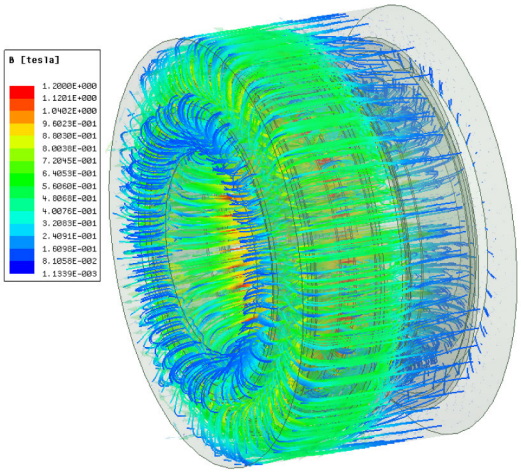

(b)

FIGURE 3. (a) The main electric and magnetic part of the motor and (b) 3D FEM simulation to flux distribution.

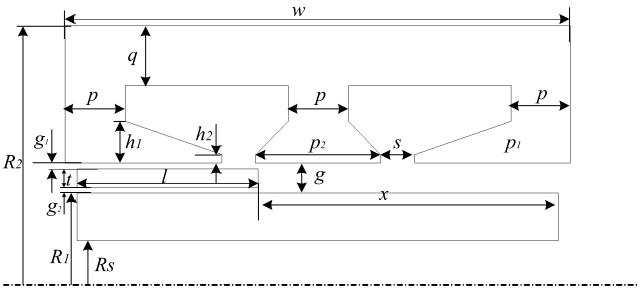

FIGURE 4. The half section scheme of the main structure.

reaction can reflect the influences of the electric load of the motor. These parameters can be analyzed and adjusted by FEM to predict the performance of the motor accurately. In this section, the basic parameters including the mechanical dimensions of the motor are analyzed and evaluated by the following equations. This is the first step to design a new motor.

A. OPEN CIRCUIT FLUX ANALYSIS

The flux line distributions generated by the PM are shown in Figure 5 when the moving PM locates at different positions. It can be seen that the flux lines are closed along with the E-core stator, the air gap and the back iron. According to the

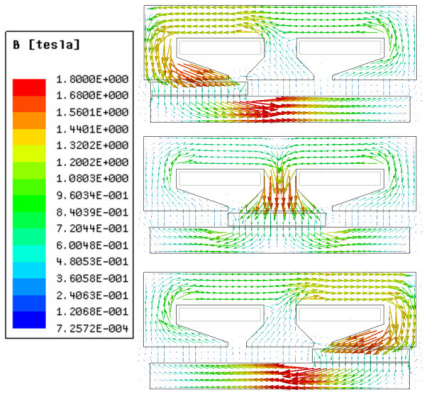

FIGURE 5. The flux distributions when the moving PM locates at (a) the left side, (b) in the middle part and (c)at the right side of the iron core.

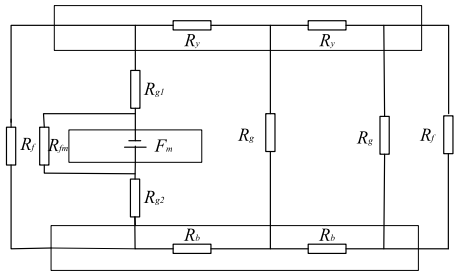

FIGURE 6. Equivalent magnetic circuit of the motor according to the half sectional scheme.

flux line figure, the equivalent magnetic circuit of the motor can be plotted as shown in Figure 6 when the coils of the motor are not excited, neglecting local saturation condition. In this figure, *Ry* and *Rs* are the magnetic reluctance of the yoke of the E-core stator and the back iron. R_f is the magnetic reluctance reflecting the fringing effect of the E-core stator and the back iron. R_{fm} is the magnetic reluctance reflecting the fringing effect of the PM. Both R_f and R_{fm} can be regarded as the factors causing flux leakage to the PM. F_m signifies the magnetic motive force (MMF) generated by the PM. In order to determine the PM size easily, the fringing effect cannot be taken into account in the first step. Assuming that the magnetic permeability of the E-core stator and the back iron is infinite, the magnetic circuit of Figure 6 can be simplified as Figure 7. The following equations can be obtained according to magnetic circuit laws..

$$\emptyset_g = \frac{F_m}{R_{g1} + R_{g2} + \frac{1}{2}R_g} \tag{5}$$

$$R_{g1} = \frac{g1}{\mu_0 l D_1} \tag{6}$$

$$R_{g2} = \frac{g2}{\mu_0 l D_2} \tag{7}$$

$$R_g = \frac{2g}{\mu_0 (w - l) D_3} \tag{8}$$

where D1, D2, and D3 represent the average circular length of these air gaps. As the magnetic flux through the air gaps and the PM are nearly equal, shown by (12), the size of the

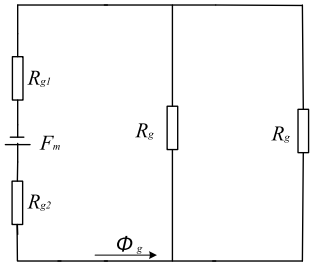

FIGURE 7. Simplified magnetic circuit for the theoretical analysis.

PM can be calculated by the following equations

$$\begin{cases} H_m t = H_{g_1} g_1 + H_{g_2} g_2 + H_g g + F_{drop} \\ B_m A_m = B_{g_1} A_{g_1} K_{g_1} = B_{g_2} A_{g_2} K_{g_2} = B_g A_g K_g \end{cases} \tag{9}$$

where H_m, H_{g_1}, H_{g_2} and H_g are magnetic intensity in the PM, air gap g_1, g_2 and g respectively. F_{drop} represents the magnet motive force drop produce by the iron cores of the magnetic circuit. B_m, B_{g_1}, B_{g_2} and B_g are magnetic flux density in the PM, air gaps g_1, g_2 and g respectively.

A_m, A_{g_1}, A_{g_2} and A_g are sectional maps of the PM, air gaps g_1, g_2 and g respectively. K_{g_1}, K_{g_2}, K_g are flux leakage coefficients. In order to simply calculation steps to obtain the size of the motor, the magnetic motive force and the flux leakage can be negligible firstly. The magnetic motive force drop and the flux leakages can be calculated according to the magnetic circuit analysis later. Then, the equation can be expressed as

$$\begin{cases} H_m t = H_{g_1} g_1 + H_{g_2} g_2 + H_g g \\ B_m A_m = B_{g_1} A_{g_1} = B_{g_2} A_{g_2} = B_g A_g \end{cases} \tag{10}$$

According to Figure 4, the sectional maps of the PM, the air gap g_1 and the air gap g_2 are equal.

$$A_m = A_{g_1} = A_{g_2} \tag{11}$$

Therefore,

$$B_m = B_{g_1} = B_{g_2} \tag{12}$$

The permeability in the PM and the air gaps is nearly identical with μ_0, then the following equations can be obtained.

$$H_m = H_{g_1} = H_{g_2} \tag{13}$$

$$\frac{B_g}{B_m} = \frac{l}{w - l} \tag{14}$$

The size of the PM can be calculated by

$$l = \frac{B_g \cdot w}{B_g + B_m} \tag{15}$$

$$t = g_1 + g_2 + \frac{l}{w - l} \cdot g \tag{16}$$

The yoke thickness and the pole width of the E-core stator can be designed by the following equations.

$$p = \frac{\emptyset_g}{2\pi(R_1 + g + h_1)B_m} \tag{17}$$

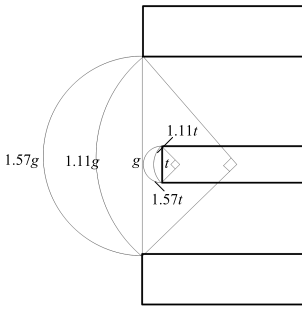

FIGURE 8. Magnetic paths for the fringing effect to the PM and the iron cores.

$$q = R_2 - \sqrt{R_2^2 - \frac{\emptyset_g}{\pi B_m}} \tag{18}$$

The magnetic motive force drop in the iron cores F_{drop} and the flux leakage effect of the motor also need to be taken into account. F_{drop} depends on the magnetic reluctances of the yoke and poles of the E-core stator and the back iron of the mover. These magnetic reluctance can be derived by the parameters of the iron cores and their relative permeability. The fringing effects on the PM and the soft material cores of the motor need to be considered. According to Figure 6, the fringing effect can be plotted as shown in Figure 8. The fringing magnetic reluctances can be calculated. The longest arc is a half-circle with the diameter of g, the length will be 1.57 times of the diameter. The second arc is a quarter of a circle shown in Figure 8 and the length of the second arc can be calculated by equation (19).

$$l' = \frac{\pi}{2} \cdot \frac{g}{2 \cdot sin\frac{\pi}{4}} = \frac{\pi}{2} \cdot \frac{g}{\sqrt{2}} \tag{19}$$

The average length of the fringing magnetic path of the soft material core will be

$$l_{R_f} = \frac{1}{3}(1.57g + 1.11g + g) \tag{20}$$

The average section map of the fringing flux form the E-core stator to the back iron can be

$$S_{av} = \frac{V}{l_{R_f}} \tag{21}$$

where V is the volume occupied by the fringing flux lines which can be approximately a half ring with the diameter of g. The fringing magnetic reluctance is calculated as 3.85 times of air gap magnetic reluctance. As the magnetic reluctance in the PM is tremendous, the average fringing magnetic path of the PM can be calculated as

$$l_{R_{fm}} = \frac{1}{2}(1.57t + 1.11t) \tag{22}$$

The flux tube volume is a half hollow ring with the diameter of t. The fringing magnetic reluctance is shown in Figure 8.

If the PM size is determined, the flux density in the air gaps needs to be modified after obtaining the fringing effects of the motor.

$$B_g A_g = B_m A_m K_f \tag{23}$$

where K_f is a coefficient to the fringing effect of the motor and it can be calculated by

$$K_f = \frac{R_{e2}}{R_{e1}} \tag{24}$$

R_{e2} and R_{e1} are magnetic reluctance of equivalent magnetic circuits in Figure 7 and Figure 6, respectively.

$$R_{e2} = R_{g1} + R_{g2} + \frac{1}{2}R_g \tag{25}$$

$$R_{e1} = R_{fm}//(R_{g1} + R_{g2} + (R_f//(R_g//(2R_y + 2R_b + R_g//R_f)))) \tag{26}$$

The symbol // signifies that the reluctances are connected in parallel.

$$R_f = \frac{g}{\mu_0 l_{Rf} D_3} \tag{27}$$

$$R_{fm} = \frac{t}{\mu_0 l_{R_{fm}} D_3} \tag{28}$$

$$R_b = \frac{w}{2\pi\mu_0\mu_r\left(R_1^2 - R_s^2\right)} \tag{29}$$

$$R_y = \frac{R_2 - g - R_1}{3\pi\mu_0\mu_r p(R_2 + g + R_1)} + \frac{w - 3p}{2\pi\mu_0\mu_r\left(R_2^2 - (R_2 - q)^2\right)} \tag{30}$$

The linear force output of the motor can be derived by the change of the magnetic flux through in the E-core stator.

$$F = N_c I\frac{d\emptyset}{dx} = 2\pi N_c I B_{g_1}(R_1 + g) \tag{31}$$

where N_c is the turns of a coil in the E-core stator. I is the current flowing along the coil. x is the displacement of the mover and $\emptyset$ denotes the flux of the E-core stator. The force constant of the motor can be obtained.

$$k_v = 2\pi N_c B_{g_1}(R_1 + g) \tag{32}$$

It can be seen that the constant of the motor mainly depends on the magnetic flux density in the air gap, the radium of the mover and the coil turns of the stator. The copper loss and the core loss of the motor can be estimated by the equations as follows.

$$p_{cu} = 2\frac{\rho l_a}{A_s K_p}(N_c I)^2 \tag{33}$$

$$p_{Fe} = p_h + p_e = K_h f B_m^2 + K_e(f B_m)^2 \tag{34}$$

K_h and K_e are 0.08 and 0.0004. ρ is the resistivity of copper. l_a is the average length of the coil in one slot of the E-core stator. A_s and K_p are the area of the slot and the package factor of the coil to the slot. If the velocity of the mover is determined, the efficiency η of the motor can be estimated according to the equations (34).

$$\eta = \frac{F \cdot v}{F \cdot v + p_{cu} + p_{Fe}} \tag{35}$$

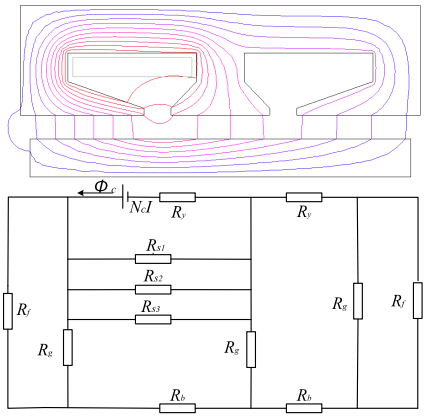

FIGURE 9. The magnetic path when one coil of the motor is excited and its equivalent magnetic model.

B. ARMATURE REACTION

The yoke thickness and the pole width of the E-core stator need to be redesigned if the coil is excited. As shown in Figure 9, the section view of flux path for the current carrying coil and its equivalent magnetic circuit are given, considering the leakage flux paths including R_{s1}, R_{s2} and R_{s3}, respectively. They can be estimated by the following equations.

$$R_{s1} = \frac{\frac{w-3p}{2} + s}{2\mu_0\pi[(R_1 + g + h_1)^2 - (R_1 + g + h_2)^2]} \tag{36}$$

$$R_{s2} = \frac{s}{\mu_0\pi[(R_1 + g + h_2)^2 - (R_1 + g)^2]} \tag{37}$$

$$R_{s3} = 3.85 \times R_{s2} \tag{38}$$

According to Figure 9, the total magnetic reluctance to the current-carrying coil can be calculated as

$$R = R_y + (R_f//R_g + R_b + R_{s1}//R_{s2}//R_{s3})//(R_y + R_f//R_g + R_b)//R_g \tag{39}$$

$$\emptyset_c = \frac{N_c I}{R} \tag{40}$$

To avoid the local saturation of the motor, the yoke thickness and the pole width of the E-core stator can be redesigned as

$$p = \frac{\max(\emptyset_g, \emptyset_c)}{2\pi(R_1 + g + h_1)B_m} \tag{41}$$

$$q = R_2 - \sqrt{R_2^2 - \frac{\max(\emptyset_g, \emptyset_c)}{\pi B_m}} \tag{42}$$

IV. OPTIMIZATION BY FEM SIMULATION

The primitive size and parameters can be calculated according to the theoretical equations. If the specifications of the motor are needed for practical manufacturing, we can calculate these parameters and mechanical dimensions accurately by FEM and this procedure can be regarded as an assistant design of electric machines because it calculates these parameters more precisely than the rough manual calculation. In order to improve the force output and reduce the force

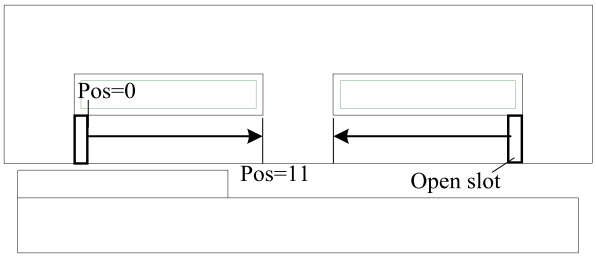

FIGURE 10. The premitive structure of the E-core stator and the moving directons of the open slots when optimizing their positions.

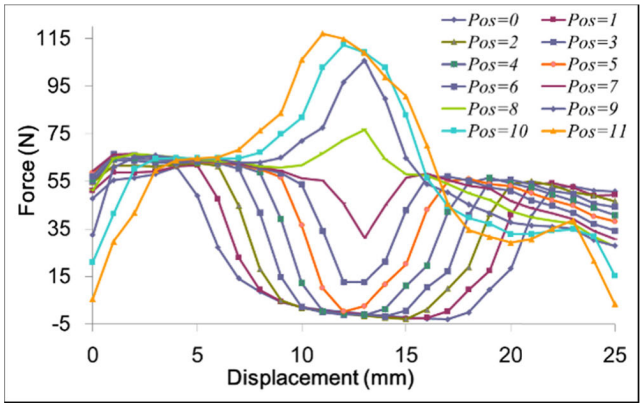

FIGURE 11. The force output curves when the slots move to different positions.

output ripple when the mover aligns with the central tooth of the stator, the teeth shape of the stator and the thickness of the PM should be optimized for this motor. In this section, some parameters are analyzed to obtain a better performance for the motor.

A. INFLUENCE OF TOOTH STRUCTURE

The length of the open slot is 3 mm and two open slots are located against the left tooth and the right tooth of the E-core stator, as shown in Figure 10. The position shown in the figure is defined as the original place of the slots. The linear force profiles of the moving PM in the entire stroke from 0 to 25 mm are calculated by FEM when the slots move to the central tooth of the stator. According to the force profiles in Figure 11, the linear force of the PM undergoes a bowl-shaped curve during the stroke when the slot position is zero, with force output approaching 55 N at the beginning displacements of 3 mm and dropping sharply to a value that is approximately minus 5 N, finally climbing to 55N at the end of displacement. This force characteristic cannot meet the force requirement of a linear motor because it has a negative part during the stroke. This negative part disappears after the slots move to the position of 6 mm. However, there is a positive force ripple after the slot position exceeds 8 mm and this ripple becomes larger afterward. Therefore, the optimal slot position could be selected as 7 mm to 8 mm for this motor under the previous design procedures.

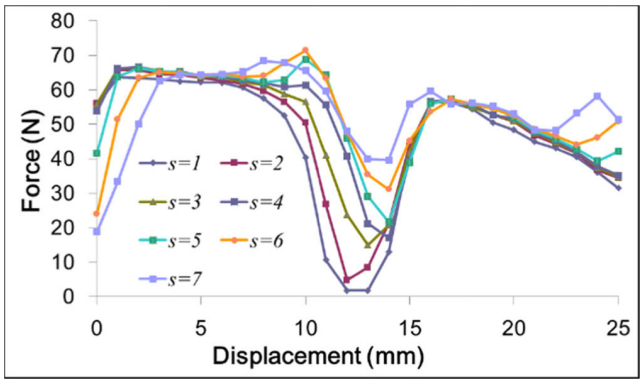

FIGURE 12. The force profiles to the varied values of s shown in Figure 4.

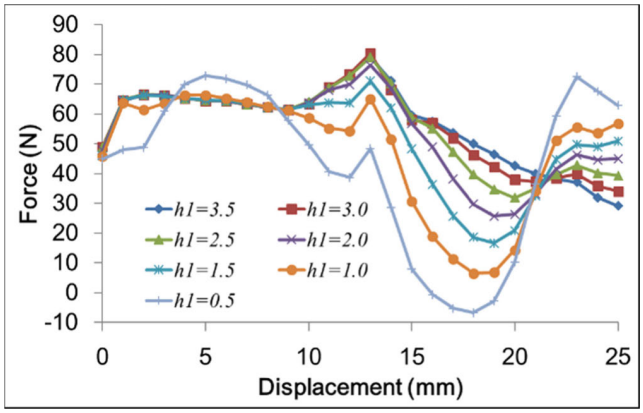

FIGURE 13. The force characteristics of the motor respects to different heights of *h1*.

If the slot is located at the position of 7 mm and the length of the slot *s* increases from 1 mm to 7 mm, the linear force output profiles are plotted in Figure12. The linear force ripple becomes smaller with the increase of the slot length. It suggests that the slot approaching the central tooth of the E-core stator can improve the force output performance of the motor, but the force output at the beginning displacement will decrease if the slot length increases. So, the slot length could be chosen between 2 mm to 5 mm for this motor for the first stage.

Apart from the influence on the force ripple from the slot length, the height of h1 can also put a significant impact on the force ripple. As shown in Figure 13, the force ripple will increase with the decrease of the height, especially for the displacements between 12.5 mm to 25 mm. This is mainly caused by the local saturation of the E-core stator due to the decrease of the height. However, increasing the height of h1 could improve the mass of the E-core stator and then the whole mass of the motor will be increased also. In order to avoid the local saturation, the tooth shape for the motor can be designed as a triangle style finally.

B. PM SIZE

After optimized the teeth shape of the motor, the size of the PM should also be optimized again. In Figure 14, when

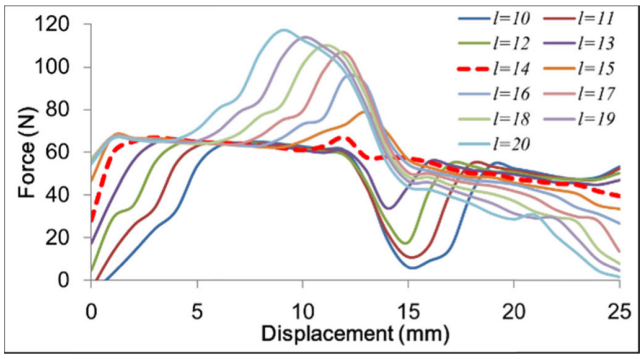

FIGURE 14. The optimized force outputs to the length of th PM.

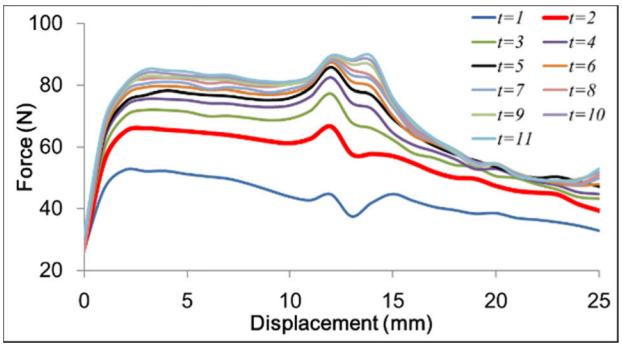

FIGURE 15. The force outputs of the motor to different PM thicknesses.

the length of the PM (l) changes from 10 mm to 20 mm, the force output profiles are obtained. For this motor, if the PM length is less than 14 mm the force output will experience a negative part after the PM displacement exceeding 12.5 mm. If the PM length is larger than 14 mm, the force output curve will become a quasi-sinusoidal waveform and the peak value can be up to 120 N. As the current following direction is a constant during one stroke and the force ripple should be limited for the LOM, the PM length is selected as 14 mm finally.

The thickness of the PM also put influence on the force output of the motor, as shown in Figure 15. When air gap1 and air gap2 are 0.3 mm and the thickness of the PM increases from 1 mm to 11 mm, the force profiles are given in Figure 15. The force output of the motor will be improved with the increase of the thickness. However, when the thickness exceeds 3 mm, the force output can increase slightly due to the limited size of the E-core stator and excitations for the designed motor. The PM thickness for the motor is 2 mm according to the previous design size of the E-core stator and power output of the motor.

Considering the electric parameters of the motor, the thickness of the PM needs to be designed precisely to get rid of fatal demagnetization of the PM. If the flux leakage of the motor is ignored and the demagnetization is totally produced by one coil, the thickness of the PM has to meet the following equation.

$$t \geq \frac{NcI}{H_m} \quad (42)$$

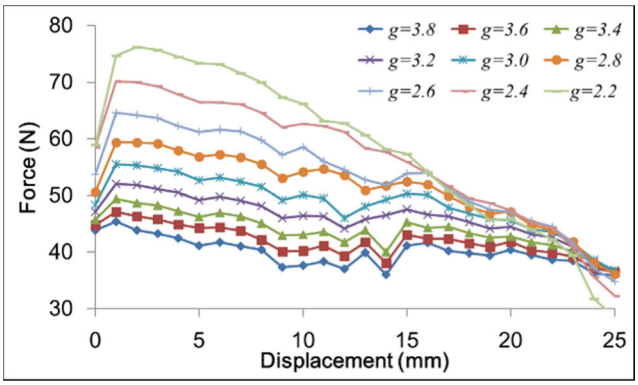

FIGURE 16. Force characteristics of the motor respect to varied air gap lengths.

H_m is the magnetic intensity that is within the optimal operating area of the PM and this value is also influenced by the ambient temperature of the PM in the motor.

C. AIR GAP LENGTH

The air gap length g can change the force output performance of the motor. When the air gap increases from 2.2 mm to 3.8 mm, the force outputs of the motor are flatter during the stroke, as shown in Figure 16. The maximum force output at the beginning position is nearly double times than that at the ending position when the air gap is 2.2 mm. Although the peak value of the force output is improved by decreasing the air gap length, the force output varies dramatically during one stroke under the rated current excitation and the manufacturing process could also become more diffident. The air gap length of the motor can be selected according to the requirements of practical applications. In this study, the air gap is selected as 2.6 mm for the designed motor.

D. COIL CONNECTION

The force output profiles under different excitation currents are obtained after finishing the optimization. The force outputs in the entire stroke are given in Figure 17 when the two coils of the E-core stator are connected in series with an identical current flowing direction. The linear force outputs are nearly proportional to the excitation currents and the force curves are nearly horizontal lines in addition to slight fluctuations in the central part. The average force output can exceed 60 N at rated current excitation.

If the two coils are excited separately, the force output profiles are obtained by FEM as shown in Figure 18. The force outputs in the displacements at the beginning to the 10 mm can keep constant values and then decrease gradually to zero at the position of 15 mm. Interesting, the force outputs generated by another coil with an identical current excitation are zero during the distance from 0 to 10 mm and increase to constant values at the position 13 mm. During the displacement of 10 mm to 15 mm, there are two force outputs simultaneously if the two currents of the coils are controlled

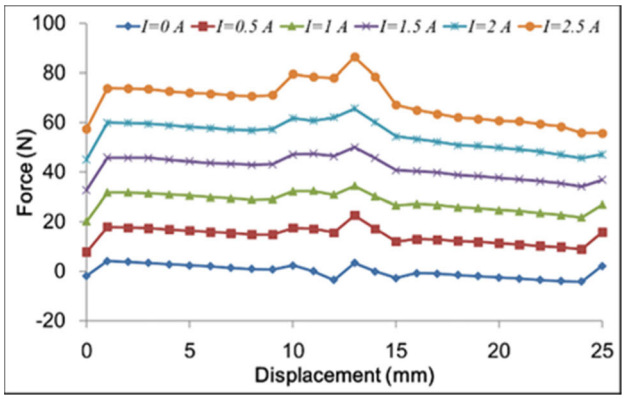

FIGURE 17. Optimized force outputs during a stroke under different current excitations.

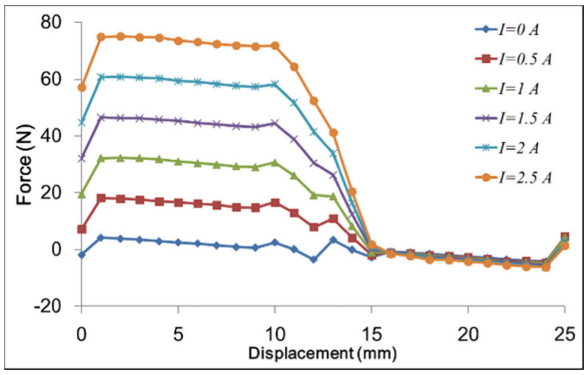

(a)The force output profiles when one coil is excited with different current levels.

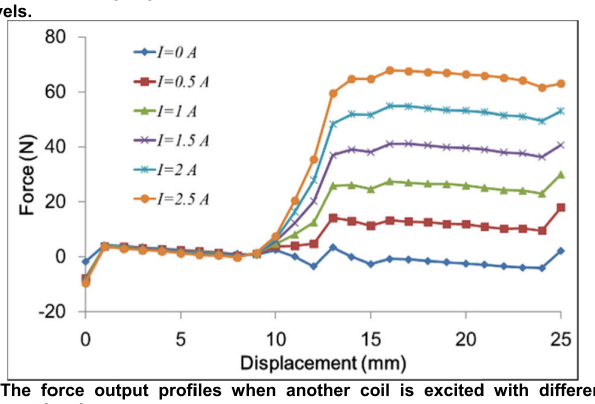

(b)The force output profiles when another coil is excited with different current levels.

FIGURE 18. (a) The force output profiles when one coil is excited with different current levels and (b) when another coil is excited.

at the same time. A comparison of some parameters for the optimized motor is given in Table 3. As there are still a lot of parameters that are not taken into account by above optimizations, these optimized values given in this table could be suboptimal parameters for the motor.

V. EXPERIMENTAL RESULTS

A. EXPERIMENTAL SETUP

The experimental platform to test the designed LOM has been built as shown in Figure 19. The whole experimental setup includes two LOMs with linear encoder, drivers for the

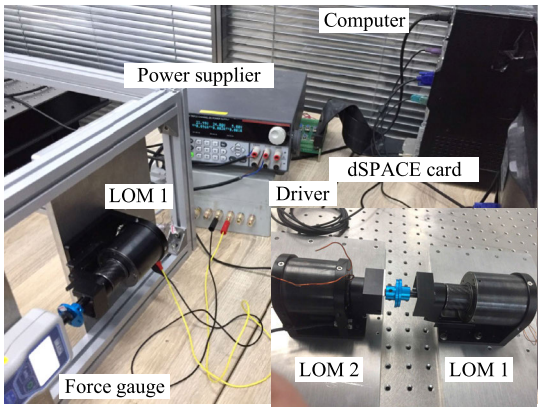

FIGURE 19. Experimental setup for testing the motor.

TABLE 3. Main optimized parameters comparison.

Parameters	Initial value	Optimized value
Slot position	6 *mm*	8 *mm*
Slot length	2 *mm*	2.8 *mm*
Slot area	40 mm^2	63 mm^2
Coil turns	170 turns	250 turns
PM length	20 *mm*	14 *mm*
PM thickness	1.5 *mm*	2 *mm*
Air gap length	2.4 *mm*	2.6 *mm*
Force output	60 *N*	65 *N*
Force ripple	20 *N*	10 *N*

motors, a power supplier, a force gauge and dSPACE card DS1104. The experiments are carried out by two steps. One is the measurement of the force outputs of the motor. The shaft of the motor is connected with the force gauge and this motor is driven by a current driver which is controlled by the dSPACE card plugging into a computer. The current of the motor can be regulated precisely according to the signal from a digital-to-analog (DAC) converter of the control card. The displacement signal of the motor is obtained by a linear decoder and this signal is a feedback to the control card. The control scheme for the motor is built by the software package MATLAB/Simulink and it can be programmed to the control card directly. Another experiment is able to test the efficiency of the LOM. The motor is connected with another linear motor that is considered as a load and this load can be controlled by the control card. Therefore, the efficiency of the motor can be tested for the motor under different reciprocating frequencies.

B. RESULTS

The force output of the motor is measured at different displacements of the mover and the motor is excited under the rated current of 2 A. The designed force outputs, the FEM results and the experimental results are compared in Figure 20 (a). Some force ripples exist in the middle part of the motion stroke of the motor and these ripples can be controlled by regulating the current of coils. The measured force outputs are a little bit less than that of FEM results. The main reason

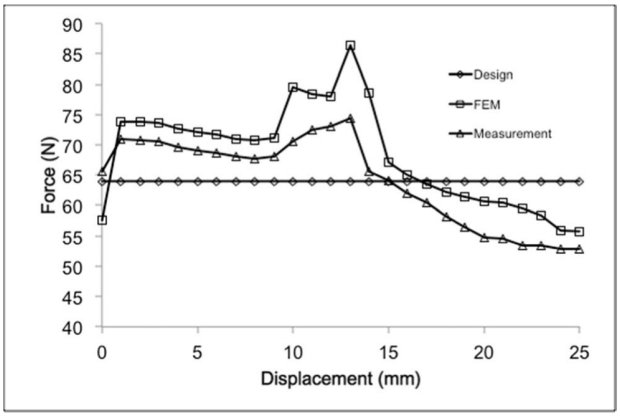

(a) Force measurement

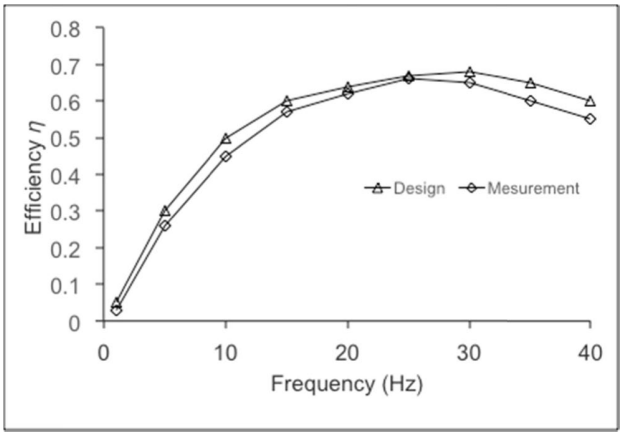

(b) Efficiency waveforms with different operation frequencies.

FIGURE 20. (a) Force outputs by theoretical calculation, FEM and practical tests and (b) the efficiency curves respect to different frequencies.

TABLE 4. Simulation and experiments.

Current	0.5 A	1 A	1.5 A	2 A	Efficiency
Simulation	15 N	30N	45 N	65 N	70%
Experiment	15 N	30N	42 N	60 N	67%

could be the flux leakage in a real application is more serious than FEM calculation. Also, the efficiency of the motor is obtained by the design and the experimental tests, as shown in Figure 20 (b). It can be seen that the efficiency of the motor experiences a parabolic curve. The efficiency is relatively low when the operation frequency of the motor is low and it will grow gradually with the increase of the frequency, reaching to 67 % at the maximum point and then going downwards slowly. The practically measured result is slightly less than that of designed calculation as some extra mechanical losses are ignored by the theoretical calculation. Generally, the measured results agree with that of the theoretical results according to Figure20.

Force outputs under different current excitations and the efficiencies from the simulation and experimental results are listed in Table 4.

VI. CONCLUSION

The paper presents a new LOM with a homopolar structure. The mechanical and working principle has been introduced firstly. The magnetic circuit of the motor is analyzed and some parameters are calculated by the design procedure. In addition, optimizations for the factors influencing the force outputs are obtained by FEM results including the shape of the tooth, the size of the PM ring and the air gap length. The experimental results show us the force characteristics of the motor and its efficiency is obtained. The main contributions of the paper include:

1) Compared with traditional studies, a new homopolar structure of the LOM is proposed and its design method is elaborated. This motor has a longer moving scope during a stroke compared with traditional LOMs with identical size.

2) The magnetic circuit analysis for the motor is given and the optimizations to improve the force outputs and reduce the force ripples have been carried out. The main specifications are obtained after optimizing the size of the motor.

3) A prototype of the motor is produced and tested. Experimental results including the force output measurement and the efficiency of the motor are obtained finally to validate the designed LOM.

The experimental results can testify the correctness of the designed procedure of the motor and the performance of the motor proves the effectiveness of the proposed structure. This motor could be widely employed in the future.

ACKNOWLEDGMENT

The authors would like to thank the Research Committee of the Hong Kong Polytechnic University under the project reference ZDAT and 845G. Y. Zou developed the analysis, hardware design and measurement. He also conducted the simulation of the work. K. W. E. Cheng was responsible for the background theory. He also provided the guidance and supervision of the study.

REFERENCES

[1] X. Xue, K. W. E. Cheng, and Z. Zhang, "Model, analysis, and application of tubular linear switched reluctance actuator for linear compressors," *IEEE Trans. Ind. Electron.*, vol. 65, no. 12, pp. 9863–9872, Dec. 2018.

[2] J. Choi, H. Lee, S. Yoo, and M. D. Noh, "Analysis and modeling of a voice-coil linear vibration motor using the method of images," *IEEE Trans. Magn.*, vol. 48, no. 11, pp. 4164–4167, Nov. 2012.

[3] L. Yan, L. Zhang, Z. Jiao, H. Hu, C.-Y. Chen, and I.-M. Chen, "Armature reaction field and inductance of coreless moving-coil tubular linear machine," *IEEE Trans. Ind. Electron.*, vol. 61, no. 12, pp. 6956–6965, Dec. 2014.

[4] I. I. Abdalla, T. Ibrahim, and N. M. Nor, "Analysis of tubular linear motors for different shapes of magnets," *IEEE Access*, vol. 6, pp. 10297–10310, 2018.

[5] X. Huang, J. Liang, B. Zhou, L. Li, and D. Gerada, "Suppressing the thrust ripple of the consequent-pole permanent magnet linear synchronous motor by two-step design," *IEEE Access*, vol. 6, pp. 32935–32944, 2018.

[6] K. H. Kim, H. I. Park, S. S. Jeong, S. M. Jang, and J. Y. Choi, "Comparison of characteristics of permanent-magnet linear oscillating actuator according to laminated method of stator core," *IEEE Trans. Appl. Supercond.*, vol. 26, no. 4, Jun. 2016, Art. no. 5201704.

[7] C.-W. Kim, G.-H. Jang, S.-W. Seo, I.-J. Yoon, S.-H. Lee, S.-S. Jeong, and J.-Y. Choi, "Comparison of electromagnetic and dynamic characteristics of linear oscillating actuators with rare-earth and ferrite magnets," *IEEE Trans. Magn.*, vol. 55, no. 7, Jul. 2019, Art. no. 8203204.

[8] J. Wang, D. Howe, and Z. Lin, "Design optimization of short-stroke single-phase tubular permanent-magnet motor for refrigeration applications," *IEEE Trans. Ind. Electron.*, vol. 57, no. 1, pp. 327–334, Jan. 2010.
[9] Z. Q. Zhu, X. Chen, D. Howe, and S. Iwasaki, "Electromagnetic modeling of a novel linear oscillating actuator," *IEEE Trans. Magn.*, vol. 44, no. 11, pp. 3855–3858, Nov. 2008.
[10] X. Chen and Z. Q. Zhu, "Analytical determination of optimal split ratio of E-core permanent magnet linear oscillating actuators," *IEEE Trans. Ind. Appl.*, vol. 47, no. 1, pp. 25–33, Jan./Feb. 2011.
[11] Y. Asai, T. Ota, T. Yamamoto, and K. Hirata, "Proposed of novel linear oscillating actuator's structure using topology optimization," *IEEE Trans. Magn.*, vol. 53, no. 6, Jun. 2017, Art. no. 8203204.
[12] J. Sun, C. Y. Luo, and S. Xu, "Improvement of tubular linear oscillating actuators by using end ferromagnetic pole pieces," *IEEE Trans. Ener. Conver.*, vol. 33, no. 4, pp. 1686–1691, Dec. 2018.
[13] A. Hassan, A. Bijanzad, and I. Lazoglu, "Dynamic analysis of a novel moving magnet linear actuator," *IEEE Trans. Ind. Electron.*, vol. 64, no. 5, pp. 3758–3766, May 2017.
[14] Z. Q. Zhu and X. Chen, "Analysis of an E-core interior permanent magnet linear oscillating actuator," *IEEE Trans. Magn.*, vol. 45, no. 10, pp. 4384–4387, Oct. 2009.
[15] Q. Lu, M. Yu, Y. Ye, Y. Fang, and J. Zhu, "Thrust force of novel PM transverse flux linear oscillating actuators with moving magnet," *IEEE Trans. Magn.*, vol. 47, no. 10, pp. 4211–4214, Oct. 2011.
[16] X. Li, W. Xu, C. Ye, and I. Boldea, "Comparative study of transversal-flux permanent-magnetic linear oscillatory machines for compressor," *IEEE Trans. Ind. Electron.*, vol. 65, no. 9, pp. 7437–7446, Sep. 2018.
[17] G. Lei, T. Wang, J. Zhu, Y. Guo, and S. Wang, "System-level design optimization method for electrical drive systems-robust approach," *IEEE Trans. Ind. Electron.*, vol. 62, no. 8, pp. 4702–4713, Aug. 2015.
[18] X. Zhu, Z. Xiang, L. Quan, W. Wu, and Y. Du , "Multimode optimization design methodology for a flux-controllable stator permanent magnet memory motor considering driving cycles," *IEEE Trans. Ind. Electron.*, vol. 65, no. 7, pp. 5353–5365, Jul. 2018.
[19] X. Zhu, J. Huang, L. Quan, Z. Xiang, and B. Shi, "Comprehensive sensitivity analysis and multiobjective optimization research of permanent magnet flux-intensifying motors," *IEEE Trans. Ind. Electron.*, vol. 66, no. 4, pp. 2613–2627, Apr. 2019.

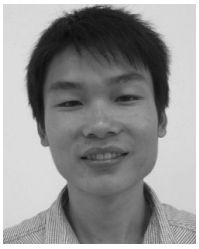

YU ZOU received the B.S. degree from Hubei University, in 2010, and the master's degree from the College of Mechatronics and Control Engineering, Shenzhen University, in 2013. He is currently pursuing the Ph.D. degree with The Hong Kong Polytechnic University.

KA WAI ERIC CHENG received the B.Sc. and Ph.D. degrees from the University of Bath, Bath, U.K., in 1987 and 1990, respectively. Before joining The Hong Kong Polytechnic University, Hong Kong, in 1997, he was with Lucas Aerospace, London, U.K., as a Principal Engineer. He is currently a Professor and the Director of the Power Electronics Research Centre, Department of Electrical Engineering, Faculty of Engineering, The Hong Kong Polytechnic University. He has authored or coauthored more than 400 articles and seven books. His research interests include all aspects of power electronics, motor drives, electromagnetic interference, electric vehicles, battery management, and energy saving. Dr. Cheng was a recipient of the Institution of Electrical Engineers Sebastian Z De Ferranti Premium Award, in 1995; the Outstanding Consultancy Award, in 2000; the Faculty Merit Award for Best Teaching from The Hong Kong Polytechnic University, in 2003; the Faculty Engineering Industrial and Engineering Services Grant Achievement Award, in 2006; the Brussels Innova Energy Gold Medal with Mention, in 2007; the Consumer Product Design Award, in 2008; the Electric Vehicle Team Merit Award of the Faculty, in 2009; the Geneva Invention Expo Silver Medal, in 2011; the Eco Star Award, in 2012; the Gold Prize at Seoul International Invention Fair, in 2015; the iCAN Gold Medal at Canada, in 2016; and the Gold Award of HK Innovation and Technology, in 2017.